Stem Cell Reports
Article
ISSCR
OPEN ACCESS

Transplantation of Embryonic and Induced Pluripotent Stem Cell-Derived 3D Retinal Sheets into Retinal Degenerative Mice

Juthaporn Assawachananont,[1,4] Michiko Mandai,[1,*] Satoshi Okamoto,[1,5] Chikako Yamada,[1] Mototsugu Eiraku,[2] Shigenobu Yonemura,[3] Yoshiki Sasai,[2] and Masayo Takahashi[1]
[1]Laboratory for Retinal Regeneration
[2]Organogenesis and Neurogenesis Group
[3]Electron Microscope Laboratory
RIKEN Center for Developmental Biology, Kobe 650-0047, Japan
[4]Graduate School of Medicine, Kyoto University, Kyoto 606-8501, Japan
[5]Department of Physiology, Keio University School of Medicine, Tokyo 160-8582, Japan
*Correspondence: mmandai@cdb.riken.jp
http://dx.doi.org/10.1016/j.stemcr.2014.03.011

SUMMARY

In this article, we show that mouse embryonic stem cell- or induced pluripotent stem cell-derived 3D retinal tissue developed a structured outer nuclear layer (ONL) with complete inner and outer segments even in an advanced retinal degeneration model (rd1) that lacked ONL. We also observed host-graft synaptic connections by immunohistochemistry. This study provides a "proof of concept" for retinal sheet transplantation therapy for advanced retinal degenerative diseases.

INTRODUCTION

Retinitis pigmentosa (RP) is a group of genetic diseases that are primarily characterized by degeneration of photoreceptors. More than 40 genes have been implicated in RP and hereditary patterns, and pathogenesis differs according to the causal gene or mutation (Ferrari et al., 2011). There is currently no effective therapy for RP, with the exception of Leber's congenital amaurosis, a disease that is caused by mutation of RPE-65 and is currently under clinical trials for possible gene therapies (Jacobson et al., 2012). However, gene therapies are not adequate for advanced stages of RP with severe photoreceptor loss, and there are still many cases of RP in which causal genes have not been determined. Although artificial retinas could offer another treatment option, this step can only be considered for severely advanced RP cases with total vision loss (Humayun et al., 2012).

Therapeutic cell transplantation has re-emerged as a promising treatment for RP in the last decade. Transplantation of postmitotic rod precursors has shown integration into host retinas and functional recovery (MacLaren et al., 2006; Pearson et al., 2012). However, successful cell integration is only observed in host retinas that retain their structured outer nuclear layer (ONL). There is limited evidence showing that cell transplantation restores vision when transplanted into eyes that are in advanced stages of retinal degeneration and have few remaining ONL cells (Barber et al., 2013; Mandai et al., 2012; Singh et al., 2013). In addition, unlike retinal sheet transplantation, cell transplantation cannot reconstruct the retinal layer (Gouras et al., 1992; Seiler and Aramant, 1998), and integrated cell survival decreases significantly in the long term (West et al., 2010). In contrast, long-term cell survival has been achieved via retinal sheet transplantation without immunosuppression (Ghosh et al., 1999; Gouras et al., 1994; Hambright et al., 2012). We previously observed successful integration of transplanted photoreceptor cells with correct polarity in an advanced retinal degeneration model, but the cells were unable to survive for >6 months (Mandai et al., 2012). In addition, because the developmental stage of graft cells is a key issue in transplantation (MacLaren et al., 2006), embryonic or early postnatal retina is not a practical cellular source for clinical applications due to ethical issues and the inherent difficulty of selecting tissues or cells at specific developmental (ontogenetic) stages adequate for transplantation.

Currently, two potential cellular sources for therapeutic transplantation are embryonic stem cells (ESCs) and induced pluripotent stem cells (iPSCs) (Takahashi and Yamanaka, 2006). Although ESC-derived retinal tissues may have low antigenicity, iPSC-derived retinal tissues have an explicit advantage in autologous cell therapy. Several groups, including ours, have reported the differentiation of retinal cells from both mouse and human ESCs and iPSCs (Hirami et al., 2009; Ikeda et al., 2005; Lamba et al., 2006; Meyer et al., 2009; Osakada et al., 2008). Successful transplantation of dissociated ESC- and iPSC-derived retinal progenitor cells has also been reported (Lamba et al., 2009, 2010). However, transplantation of ESC- and iPSC-derived retinal sheets has not been thoroughly studied.

Recently, Eiraku et al. (2011) reported the creation of a self-organizing optic cup using 3D culture, which allowed

us to achieve sufficient quality, quantity, and purity of retinal tissues for grafting, as well as to prepare retinal tissue at any developmental stage. Moreover, 3D differentiation provided a choice between preparing a sheet or cell suspension for grafting (Gonzalez-Cordero et al., 2013). Thus, although cell transplantation may be more effective during early retinal degeneration (Barber et al., 2013; MacLaren et al., 2006; Pearson et al., 2012), retinal sheet transplantation may be more effective during advanced stages of retinal degeneration with few host photoreceptors or ONL, improving the incidence of structured outer segment (OS) formation and long-term cell survival (del Cerro et al., 2000; Ghosh et al., 1999; Gouras et al., 1994; Hambright et al., 2012; West et al., 2010).

In the present study, we evaluated the ability and potency of grafted 3D-differentiated ESC- or iPSC-derived retinal sheets to differentiate into various retinal cell types and mature photoreceptors that fully form OS or synapses in a model of advanced retinal degeneration with absence of ONL. In addition, we analyzed the developmental stage-dependent integration pattern of grafted retinal sheets with the possibility of making a host-graft synaptic connection. This study provides a "proof of concept" for retinal sheet transplantation therapy and contributes to the advent of more effective and lasting therapies for patients with advanced stages of retinal degeneration.

RESULTS

Efficient Generation of Neural Retina for Transplantation

First, we optimized the protocol to produce larger quantities of neural retinal tissue for transplantation using an *Rx*-KI-GFP mESC line (Osakada et al., 2008; Wataya et al., 2008). The *Rx* gene is expressed in neural retinal progenitor cells and is important for eye-field development. We modified the SFEBq protocol (Eiraku et al., 2011) by adding retinoic acid receptor antagonist (RRA) AGN193109 and increasing the knockout serum replacement (KSR) percentage from 1.5% to 5% (Figure 1A). The effect of combining RRA with the extracellular matrix (Matrigel; BD Biosciences) resulted in a higher percent yield of *Rx*-GFP+ cells compared with the control or with addition of only RRA or only Matrigel (Figure 1B). Under this protocol, *Rx*-GFP mESCs (Figure 1C) formed aggregates and expressed *Rx*-GFP at differentiation days 4–5 (DD4–5), and then around DD5–6 evaginated to form optic-vesicle-like structures. Almost all aggregates strongly expressed *Rx*-GFP on DD8, with each aggregate forming five to eight optic-vesicle-like structures (Figures 1D and 1E). Because the *Rx* gene is also expressed in the hypothalamic region of the brain (Furukawa et al., 1997), we performed immunostaining for PAX6 to confirm neural retina induction. PAX6 is crucial for eye development and is not found in the hypothalamus (Callaerts et al., 1997). All of the *Rx*+ spheres were also positive for PAX6 by immunostaining (n = 62 spheres, 4 experiments; Figures 1F–1H). PAX6 was also expressed in the neuroepithelial region outside the *Rx*-GFP+ region (Figure S1A available online). Quantitative analysis showed that the percentage of *Rx*-GFP+ cells in each of 10 spheres ranged from 25% to 71% (mean ± SD hereafter; average 60.19% ± 10.80%, n = 5 experiments; Figure 1I), and 97% ± 3.64% of the *Rx*-GFP+ population were PAX6+ (n = 3 experiments; Figure 1J), indicating that the *Rx*-GFP+ cells in our culture are almost exclusively retinal progenitors.

Reproducible Differentiation of Retinal Cells from ESCs and iPSCs

We also tested the consistency of our protocol using other two lines: *Rosa26*-tdTomato/*Rx*-GFP knockin mESCs (Muzumdar et al., 2007), which ubiquitously express tdTomato on cell membranes, and *Nrl*-GFP miPSCs (Homma et al., 2013). The *Nrl*-GFP miPSC line was generated as previously described. In *Nrl*-GFP transgenic mice, the expression of enhanced GFP was specific to rod photoreceptors and was detected shortly after terminal cell division (Akimoto et al., 2006).

First, we checked the gene-expression profile of optic vesicles cut out of a sphere differentiated from three cell lines (*Rx*-GFP mESCs, Rosa26-TdTomato *Rx*-GFP mESCs, and *Nrl*-GFP miPSCs) by RT-PCR. At DD10, *Rx* was highly expressed, whereas the pluripotency genes *Oct4* and *Nanog* were downregulated compared with their expression levels in undifferentiated mESCs and miPSCs (DD0; Figure 1K). Both mESCs and miPSCs were reproducibly differentiated into retinal organoids with optic-vesicle-like structures, with mean % aggregates of 93.54% ± 5.33% with *Rx*-GFP mESCs (range 88%–100%), 60.42% ± 14.30% with *Rosa26*-TdTomato *Rx*-GFP mESCs (range 46%–80%), and 70.21 ± 6.36% with *Nrl*-GFP miPSCs (range 66%–81%; n = 5 experiments for each cell line, 96 aggregates per experiment).

We showed that miPSCs were also induced into optic vesicles represented by well-organized retinal neuroepithelial-like layers. We observed ISL1+ cells (retinal ganglion cells) as early as DD10 (Figure 1L). On DD10, the inner limiting membrane (ILM) labeled with LAMININ was still present (Figure 1L), whereas on DD15 the ILM disappeared and the retinal ganglion cell layer was disorganized. At DD24, the outer neuroblastic layer was positive for RECOVERIN and CRX (photoreceptor progenitor; Figure 1M), and some cells had developed into mature photoreceptors identified as RHODOPSIN+ cells (Figures 1N–1Q). These retinal-like structures derived from *Nrl*-GFP miPSCs also comprised inner neuroblastic cells, amacrine cells (CALRETININ+; Figure 1N), horizontal cells (CALBINDIN+; Figure 1O),

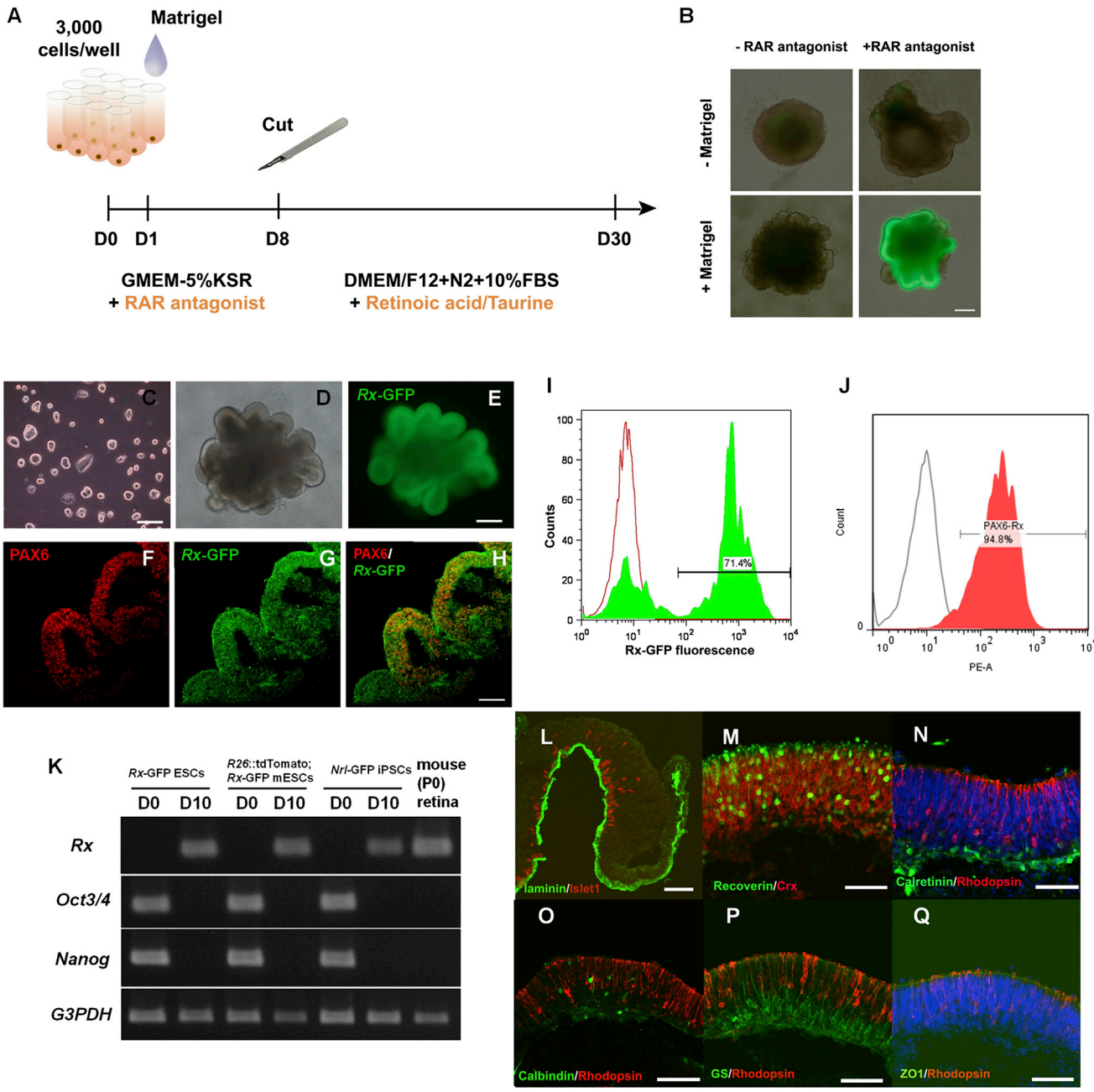

Figure 1. Efficient and Reproducible Generation of Neural Retina from mESCs and iPSCs

(A) Schematic diagram of the modified protocol used for 3D differentiation of mESC- and miPSC-derived neural retinal sheets.

(B) Enhancing effect of retinoic acid receptor antagonist on *Rx*-GFP induction.

(C) Colonies of *Rx*-GFP mESCs.

(D and E) DD8 aggregate with *Rx*-GFP optic-vesicle-like structures.

(F–H) Immunostaining of DD7 *Rx*-GFP mESC-derived neural retina shows coexpression of the *Rx*-GFP and PAX6, indicating retinal progenitors.

(I) Green histogram: percentage of *Rx*-GFP+ cells among DD9 mESC-derived spheres. Red open-peak histogram: undifferentiated *Rx*-GFP mESCs (isotype control).

(J) Red histogram: percentage of PAX6+ cells among *Rx*-GFP+ cells of DD8 mESC-derived spheres. Black open-peak histogram: isotype control. Almost all of the *Rx*+ cells were PAX6+, and PAX6 expression was observed outside the vesicles as well (Figure S1A).

(K) PCR shows downregulation of the pluripotent genes on DD10 with increased gene expression of *Rx* in all three lines tested.

(legend continued on next page)

and glia cells (GS+; Figure 1P). Detection of the external limiting membrane (ELM) was accomplished by immunolabeling with ZO1 (Figure 1Q). Thus, our results were consistent with a previous report involving mESCs (Eiraku et al., 2011). Furthermore, the ontogenic stages of differentiated tissues from mESCs and miPSCs were consistent with CRX staining detected as early as DD15, and expression of RECOVERIN and RHODOPSIN became evident in the outermost layer of the optic-vesicle-like sphere (future ONL) on DD20. These expression patterns were also consistent with those found in wild-type mouse retina: the expression patterns of RECOVERIN, CRX, CALRETININ, and RHODOPSIN on DD21 and DD24 in these tissues were similar to those observed in the developing mouse retina on postnatal days 1 and 6, respectively (Sharma et al., 2003; Figure S1B). Also, *Nrl*-GFP miPSC-derived spheres started to express *Nrl*-GFP by DD18, indicating that cells had become rod precursors (Figures 2B′ and 2D′), and the expression levels of *Nrl*-GFP gradually increased as differentiation progressed (n = 171 aggregates, 11 experiments; Figure S1C). This was consistent with the reported expression profile of *Nrl*-GFP mice (Akimoto et al., 2006), i.e., DD21 was approximately equivalent to mouse postnatal day 1 and cells younger than DD20 were considered to be embryonic retinal tissue.

mESC- and miPSC-Derived Retinal Sheets Survived and Matured in the Subretinal Space of rd1 Mice

Rd1 mice were used as a model of rapid progressive RP with end-stage retinal degeneration. In this model, most rod photoreceptor cells are lost by 3 weeks of age (Lolley et al., 1994). Retinal sheets were prepared from DD11–24 *Rx*-GFP mESC- and *Nrl*-GFP miPSC-derived aggregates (Figures 2A, 2A′, 2B, and 2B′) at the time of transplantation. *Rx*-GFP mESC- and *Nrl*-GFP miPSC-derived retinal sheets (Figures 2C, 2C′, 2D, and 2D′) were transplanted into the subretinal space of 6- to 8-week-old rd1 mice and sacrificed 2 weeks to 6 months after transplantation (Figure 2E). Both mESC- and iPSC-derived transplanted retinal sheets survived and matured under the severely degenerated rd1 retina, and RHODOPSIN+ cell masses were confined to the grafted area (Figures 2F and 2G). Next, we examined short (2–4 weeks) and midterm (1–3 months) outcomes after transplantation. The subsequent degrees of maturation and structural integrity of mESC- and iPSC-derived retinal sheets from grafts of various ages (DD11–24) were evaluated (Figure S2A). For this purpose, we categorized the degree of maturation and structural integrity of the grafts based on development after transplantation into three groups.

(1) Group A: retinal sheets with almost complete inner nuclear layer (INL) and ONL (Figures 2H–2K).
(2) Group B: retinal sheets with structured ONL and partial INL (Figure 2L).
(3) Group C: disorganized structures (Figure 2M).

In groups A and B, grafts had structured ONL with well-aligned Muller glia and an intact ELM, consistently accompanied by different degrees of inner and outer segment (IS/OS)-like structures. Group C had a disorganized glial pattern and tended to behave similarly to cell transplantation (Mandai et al., 2012).

We observed a significant difference in subsequent outcomes between the young grafts (graft age DD11–17) and older grafts (graft age DD18–24) (Figures 2N and S2A). Accordingly, young grafts (graft age DD $\leq$ 17) were still in neuroblastic states at the time of transplantation. These sheets had a better potency to develop into an almost complete retinal layer with both an inner plexiform layer (IPL)/INL and ONL (group A). We also observed structured ONL with or without INL (groups A and B), the essential part of a graft, with higher frequency in younger grafts. With grafts of DD17 or younger, in both the short and midterm posttransplantation periods, 87.5% (21/24) and 75% (22/29) of transplants developed structured ONL in groups A and B, respectively (Figures 2H–2K and 2L). The ONLs in group B formed rosette-like structures, seemingly with a loss of INL structure. Most of the DD18 or older grafts showed disorganized structures (78.57% [11/14] and 90.47% [19/21] in both the short and midterm postoperation periods, respectively; Figure 2N). Additionally, we tested whether a longer posttransplantation period (3–6 months) affected the subsequent graft integrity of the young grafts, but we observed no significant difference (Figure S2B), and many young grafts (DD11–17) showed structured ONL even after 6 months posttransplantation (Figure S2C).

mESC- and miPSC-Derived Retinal Grafts Showed Native-like IS/OS Formation in the Subretinal Space of rd1 Mice

In groups A and B, the mESC- and miPSC-derived retinal grafts with structured ONL had different degrees of

(L) Immunostaining of DD10 *Nrl*-GFP miPSC-derived neural retina for LAMININ (basement membrane) and ISLET1 (ganglion cells). (M–Q) Retina marker expression of DD24 *Nrl*-GFP miPSC-derived neural retina, rod photoreceptors (RHODOPSIN), amacrine cells (CALRETININ), horizontal cells (CALBINDIN), photoreceptor precursors (CRX, RECOVERIN), Muller glia (GS), and external limiting membrane (ZO1). All of these markers were similarly expressed in both mESCs and miPSCs, and were also correlated with the developing retina (Figures S1B and S1C). Scale bars, 200 μm (B–E) and 50 μm (F–H and L–Q).
See also Tables S1 and S2.

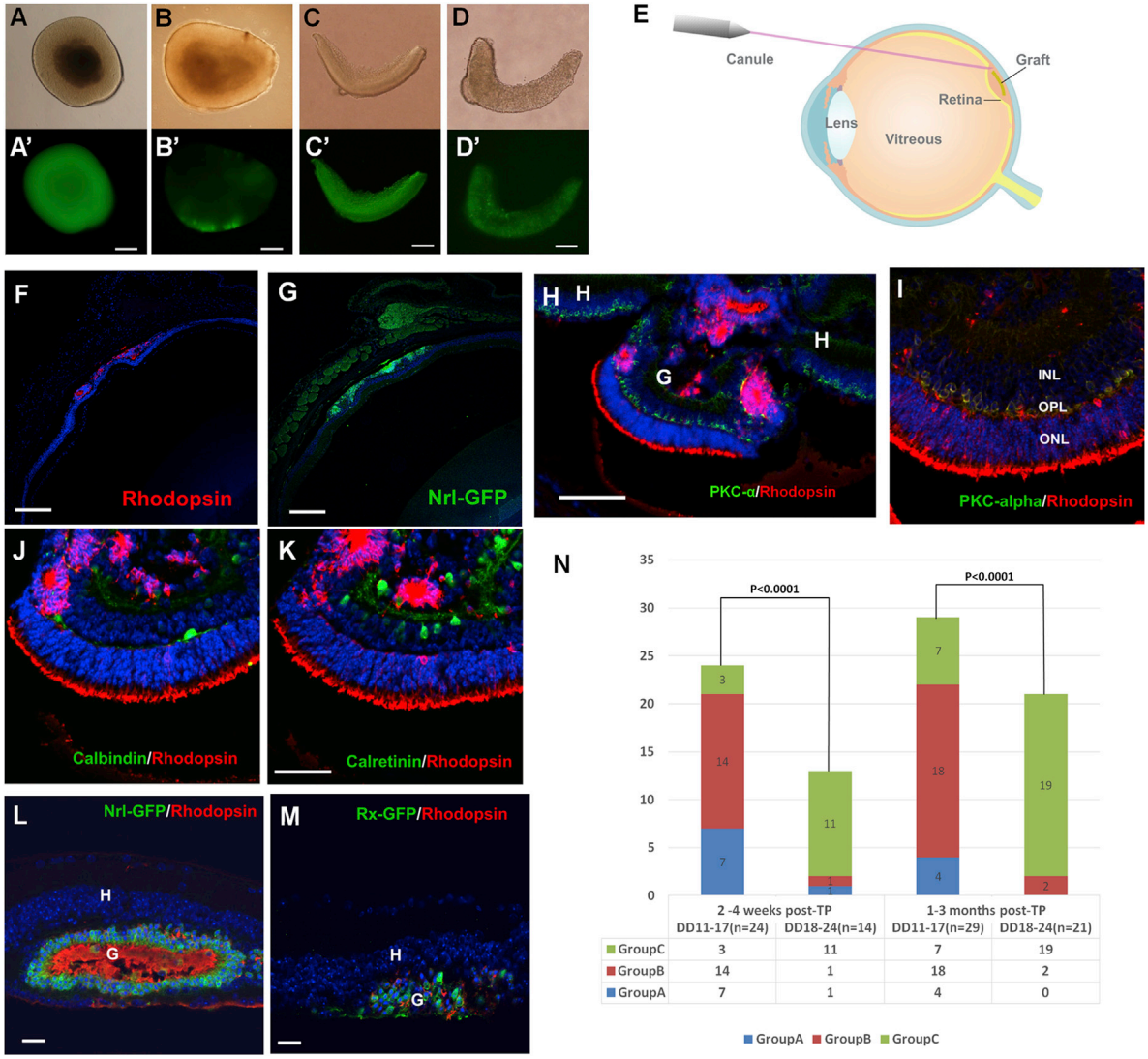

Figure 2. Transplanted Retina-like Sheets Show a Well-Developed Stratified Retinal Layer

(A) DD14 excised optic-vesicle-like tissue from *Rx*-GFP mESCs.

(B) DD18 excised optic-vesicle-like tissue from *Nrl*-GFP miPSCs with developing *Nrl*-GFP+ photoreceptor precursors from the surface area of a sphere.

(C) DD22 *Rx*-GFP mESC-derived retina sheet.

(D) DD18 *Nrl*-GFP miPSC-derived retina sheet.

(E) Scheme showing an image of subretinal transplantation.

(F and G) The DD17 *Nrl*-GFP miPSC-derived sheet survived in the subretinal space of an rd1 mouse that had no remaining photoreceptors at 3 weeks posttransplantation. The RHODOPSIN+ cell mass (F) was only present in the graft area with colocalized *Nrl*-GFP expression (G).

(H–K) The DD14 *Nrl*-GFP miPSC-derived retinal sheet developed a stratified neural retina layer that included ONL, INL, and IPL (group A).

(L) DD16 *Nrl*-GFP miPSC-derived retinal graft showed well-structured ONL (group B).

(M) DD18 *Rx*-GFP mESC-derived retinal graft in a disorganized pattern (group C).

(N) Bar graph shows the subsequent graft patterns of short (2–4 weeks) and midterm (1–3 months) posttransplantation periods, comparing young grafts (DD11–17) and older grafts (DD18–24). The subsequent graft integrity was categorized into three groups: group A, retinal sheet with INL/IPL and ONL (H–K); group B, retinal sheet with ONL and the remaining INL cells (L); and group C, disorganized structure (M). The sample numbers of each group are indicated below. H, host; G, graft; IPL, inner plexiform layer.

Scale bars, 200 μm (A–C and F-H), 100 μm (D), 50 μm (I–K), and 20 μm (L and M). See also Figure S2 and Table S1.

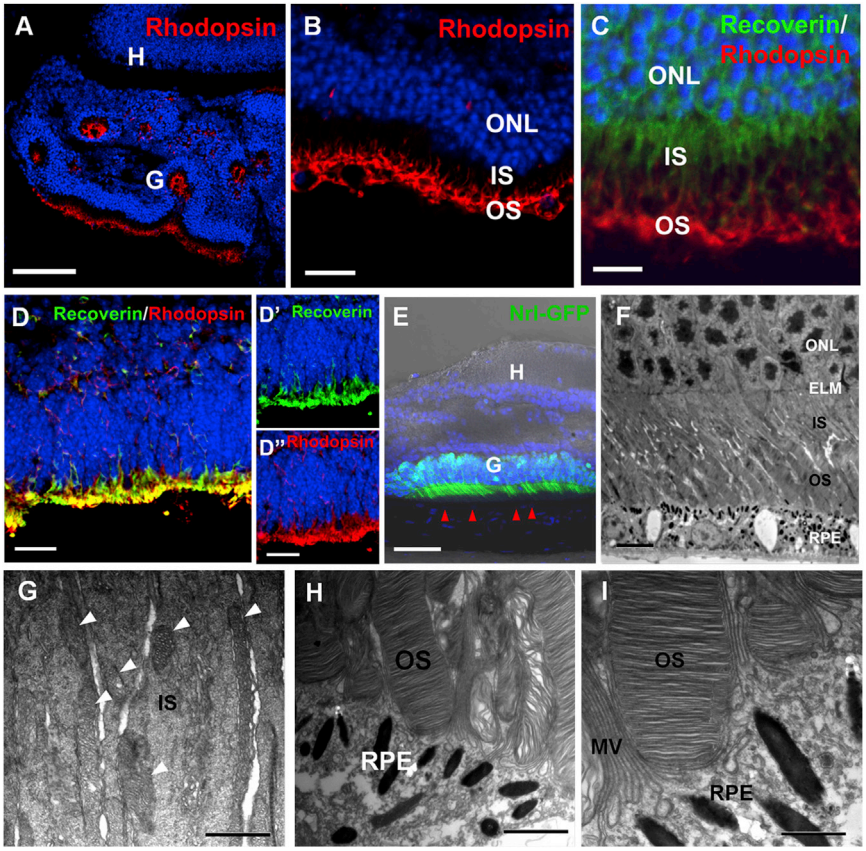

Figure 3. IS/OS Formation in Transplanted Retina-like Sheets

(A–C) DD14 *Nrl*-GFP miPSC-derived retinal graft showed IS/OS. IS was labeled with RECOVERIN; OS was labeled with RHODOPSIN (C).

(D–D″) *Rx*-GFP mESC-derived retinal culture at DD26 showed short IS/OS colabeled with RECOVERIN and RHODOPSIN.

(E–J) DD17 *Nrl*-GFP miPSC-derived retinal graft with IS/OS contact host RPE (red arrowhead) more than 4 months post-transplantation.

(F) Electron microscopy showed that rod nuclei in ONL contained a compact mass of heterochromatin, ELM, IS/OS, and RPE.

(G and H) IS with mitochondria (white arrowheads) (G) and a well-aligned stack of discs in OS on top of RPE adjacent to microvilli of RPE (H).

(I) RPE microvilli in close connection with OS. H, host; G, graft; ELM, external limiting membrane; IS, inner segment; OS, outer segment; RPE, retinal pigment epithelium; MV, microvilli.

Scale bars, 100 μm (A), 50 μm (D–D″ and E), 20 μm (B and F), 10 μm (C), 2 μm (I), and 1 μm (G and H). See also Table S1.

IS/OS formation with and without direct contact to the host retinal pigment epithelium (RPE; Figures 3A and 3E). IS/OS structures that were morphologically similar to those of the wild-type were observed from as early as 3 weeks after transplantation when in contact with host RPEs. RHODOPSIN specifically localized at the OS portion (Figures 3A and 3B), whereas RECOVERIN distributed from the OS toward the IS in the light state, and these distributions aided identification of the IS/OS development of transplanted photoreceptors (Figure 3C; Strissel et al., 2005). In contrast, even with longer differentiation cultures (>DD24), photoreceptors only showed a short, premature IS/OS-like structure or connecting cilia extending over the ELM that were colabeled with RECOVERIN and RHODOPSIN (Figures 3D–3D″). An ultrastructural analysis of some transplanted grafts after 4 months showed structured ONL of rod photoreceptors with long IS/OS structures in association with host RPE cells (Figures 3F–3I). The IS portions were found to contain mitochondria (Figure 3G), whereas the OS portions contained well-aligned, disc-like membrane stacks (Figure 3H), and these OS portions were in close association with RPE microvilli (Figure 3I).

Graft Integration with Possible Synaptic Connection

In order to evaluate the graft integration pattern, we examined the samples at 2 weeks to 3 months posttransplantation. Interestingly, we observed specific patterns of graft integration into the host retina. By immunostaining, the sites that displayed protein kinase C (PKC)-α-labeled host bipolar dendrites associated with graft photoreceptor axons were regarded as possible integration sites. The integration patterns of the grafts were typically categorized as follows:

Pattern 1: laminar interception. Nonphotoreceptor cells, mostly graft INL, were present between host INL and graft ONL, interfering with direct contact of graft photoreceptors with host cells, but very rarely graft photoreceptors could migrate and reach the host bipolar cells (Figures 4A and 4D).

Pattern 2: direct contact. Graft photoreceptors in structured ONL were adjacent to host INL (Figure 4B). In most cases, graft ONL formed rosette-like structures that directly integrated into host INL. These rosettes often had graft INL/IPL surrounding the ONL obstructing the direct photoreceptor-RPE contact (Figures 4B and 4E), but some "semi-round" incomplete rosettes allowed graft ONL to settle in the correct direction with OS pointing toward RPE (Figures 4B′, S3A, and S3A′).

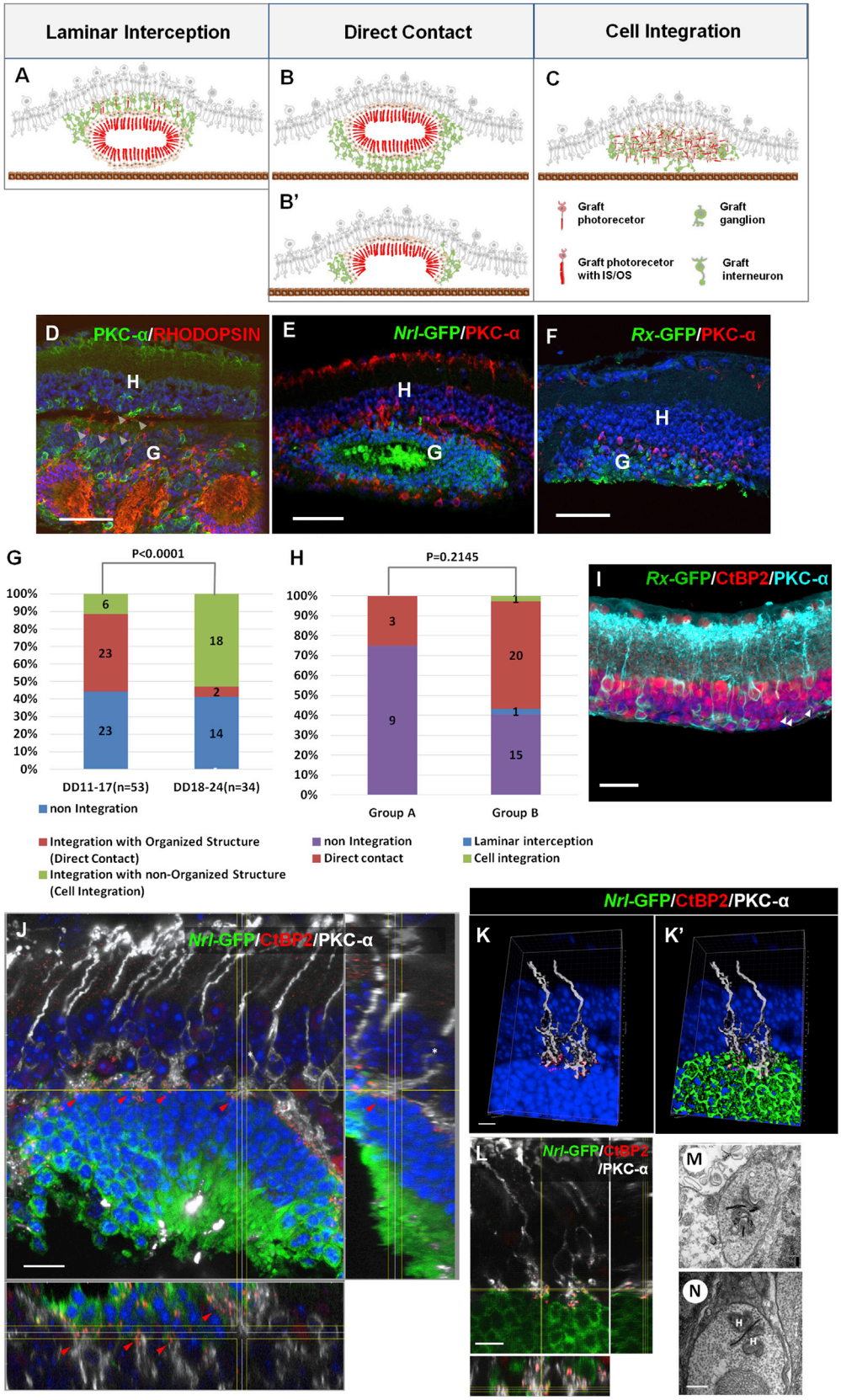

(legend on next page)

Pattern 3: cell integration. Graft ONL structure was disorganized, but photoreceptors could migrate individually into the host retina, as was observed in cell transplantation (Figures 4C and 4F).

Even though the possible integration efficiency was approximately 60% with both the young grafts (DD $\leq$ 17) and the older grafts (DD $\geq$ 18), the integration patterns were significantly different in that the young grafts integrated into the host retina mostly in a direct-contact pattern (23/53, 43.40%), whereas the older grafts that integrated into host retina rarely retained ONL structure (2/34, 4.7%), and most of the grafts became disorganized as had been observed in dissociated cell transplantation (Figure 4G). Nonintegrated patterns were seen mostly in the pattern 1 laminar interception without photoreceptor migration, or nonphotoreceptor cells located closer to the host in disorganized patterns.

Among the samples of young grafts (DD11–17), 3/10 (27.27%) in group A (complete INL+ONL) integrated with direct contact, whereas 20/32 (62.50%) in group B (partial INL+ONL) integrated with direct contact (Figure 4H), suggesting that graft ONLs accompanied by fewer INL components may have a better chance to achieve direct contact with host INL. When we closely observed these direct-contact patterns, we observed that a part of the graft ONL often looked like it was being "stripped off" from its own graft INL when the graft ONL was making direct contact with host INL cells, forcing the graft bipolar cells to be "pushed aside" (Figures S3A and S3A′). Additionally, there was no significant difference in the subsequent integration pattern between miPSC- and mESC-derived retinal grafts, indicating an equal potency of miPSCs and mESCs as graft sources. Among the samples of young grafts (DD11–17), 12/31 (38.71%) of miPSC-derived retina grafts and 11/22 (50%) of mESC-derived retinal grafts integrated with direct contact (Figure S3B).

We further examined the synaptic details of the host-graft interaction by 3D analysis using z-scan capturing of the images. We used PKC-α staining to visualize rod bipolar dendrites and CtBP2, a presynaptic protein that typically stains in a horseshoe shape at the rod terminal in the ribbon synapse (Schmitz et al., 2000). After retinal degeneration, a few CtBP2+ synaptic terminals were detected on bipolar dendrites of rd1 mice by postnatal week 6 (Figure 4I). In all of 13 direct-contact samples observed with CtBP2 immunostaining, clusters of CtBP2+ photoreceptor terminals were consistently found in the area of the host-graft interface (Figure 4J) as well as in the outer plexiform layer (OPL) within the graft. In some samples, CtBP2+ terminals of the *Nrl*-GFP+ photoreceptors were clearly seen clustering at the extending dendrite tips of host PKC-α+ bipolar cells (Figure 4J, red arrowhead). We identified these bipolar cells as host cells by tracing their axons back within the host retina. Some of these CtBP2+ terminals formed the typical horseshoe shape on host bipolar dendritic tips (Figures 4J, 4K, 4K′, and 4L; Movie S1). Also

Figure 4. Transplanted Retina-like Sheets Show Integration and Synaptic Connection with rd1 Host Retina

Schematic diagrams show three typical patterns of integration with rd1 host retina of the transplanted grafts.

(A) Pattern 1: laminar interception. Graft INL was present between host INL and graft ONL.

(B) Pattern 2: direct contact. The graft ONL was adjacent to the host INL.

(C) Pattern 3: cell integration. The graft ONL structure was disorganized, similar to what was observed for cell transplantation.

(D) A typical image of pattern 1. RHODOPSIN+ photoreceptors from DD16 *Nrl*-GFP miPSC-derived retinal sheets migrate toward the host retina (white arrowhead). H, host; G, graft.

(E) A typical image of pattern 2. DD16 *Nrl*-GFP miPSC-derived retinal sheets show structured ONL directly contacting host INL (same sample as Figure 2L). H, host; G, graft.

(F) A typical image of pattern 3. DD18 Rx-GFP mESC-derived retinal grafts show disorganized patterns similar to those observed for cell transplantation (same sample as Figure 2M). H, host; G, graft.

(G) Classification of integration patterns of surviving mESC- and iPSC-derived retinal sheets in the subretinal space of rd1 mice, comparing young grafts (DD11–17) and older grafts (DD18–24).

(H) Classification of integration patterns of surviving mESC- and iPSC-derived retinal sheets in the subretinal space of rd1 mice, comparing the structural integrity of groups A (INL+ONL) and B (ONL).

(I) A few CtBP2+ synaptic terminals remained in the area of bipolar dendrites in the nongrafted area in rd retina (arrows).

(J–L) DD11 Nrl-GFP miPSC-derived retinal sheets integrated into rd1 host retina. The graft shows dense synaptic (CtBP2) connection clusters (red arrow) between the host-graft interfaces.

(J) A representative host bipolar cell (asterisk) shows CtBP2 gathering at the tip of dendritic processes.

(K and K′) Reconstruction image of a couple of host bipolar (PKC-α) cells with CtBP2 assembled at synaptic tips (K) colocalized with *Nrl*-GFP photoreceptors (K′).

(L) Orthogonal view of the reconstructed images of K and K′ (see related images in Figures S3C, S3C′, and S3D).

(M and N) Electron micrographs show a ribbon synapse from the DD18 Rosa26-TdTomato *Rx*-GFP mESC-derived retinal graft in the graft-host interface area (M; Figures S4A–S4D) compared with the intragraft ribbon synapse from the DD17 *Nrl*-GFP miPSC-derived retinal graft (N; Figures S3E–S3J). H, horizontal cell.

Scale bars, 50 μm (D–F), 20 μm (I), 10 μm (J), 7 μm (L), 5 μm (K and K′), 500 nm (N), and 200 nm (M). See also Table S1 and Movie S1.

with Rosa26-TdTomato *Rx*-GFP mESC-derived grafts, we observed that tdTomato+ graft cells and host bipolar cells mutually extended processes across the host-graft border line (Figure S3C). Additionally, *Rx*-GFP−, PKC-α+ bipolar cells contacted CtBP2+ terminals of graft *Rx*-GFP+ photoreceptors (Figures S2D and S2D′, yellow arrow). Based on these results, we could reasonably estimate that the bipolar cells that made synapses with graft photoreceptors were host bipolar cells rather than migrating graft-derived bipolar cells. Observation of the cell integration pattern of disorganized grafts (n = 3) showed that CtBP2+ graft photoreceptor terminals (Figure S3E, yellow arrowhead) were also labeled in contact with host bipolar dendrites, although these contacts were less frequently observed compared with those seen in the direct-contact pattern (asterisk, PKC-α).

In electron micrographs, synaptic ribbons were found at the host-graft interface in a direct-contact pattern (Figures 4M, S4B, S4B′, S4C, and S4D). We also observed typical intragraft synaptic connections in the OPL area of the grafts (group A; Figures 4N and S4E–S4J). In most samples with structured or unstructured ONL, Muller gliosis as indicated by glial fibrillary acidic protein (GFAP) staining did not seem to specifically block the host-graft synaptic interaction. Typical images are shown in Figures S3F and S3G for structured ONL and disorganized graft 2 months and 40 days after transplantation, respectively.

DISCUSSION

Using a modified protocol to produce larger quantities of neural retinal cells for transplantation, we showed that transplanted 3D differentiated mESC- or miPSC-derived retinal sheets could develop to form ONL structure consisting of mature photoreceptors that were indistinguishable from those of the differentiated wild-type ONL. These transplanted photoreceptors could form complete IS/OS, a highly differentiated and complex structure, even in the subretinal space of severely degenerating host retina. Furthermore, these structured graft ONLs integrated with a direct contact to the INL of end-stage host retina that lacked ONL, where host bipolar cells and graft photoreceptor cells contacted at their terminals. It is noteworthy that miPSC-derived 3D retinal tissues have a potency equivalent to that of those derived from mESCs for transplantation purposes. After transplantation, the grafts of DD17 or younger were more efficient in forming such structured ONLs and making direct contact with host INL.

With extended culture of optic vesicles, neural retinas differentiated into retinal neurons similar to the stages of retinal cell genesis and differentiation in vivo. However, in our culture conditions, the inner neuroblastic retina tended to become loose, and the intact ILM and distinct ganglion cell layer were rarely observed after DD15. On the other hand, the outer neuroblastic layer was well developed and appeared normal. This may be due in part to the culture conditions affecting the development of INL, as seen in explant cultures (Ghosh et al., 2009). This could be advantageous for transplantation because a thicker INL graft might prevent photoreceptors from connecting with host retina. Nevertheless, grafts of DD18 or older had lower survival and a significantly higher risk of losing ONL structures after transplantation. This may be due in part to our culture conditions, tissue viability, and the differentiated tissue becoming fragile during the longer culture period. The lack of OS development in our culture also suggested that some other factors may be required for maturation of these tissues in culture.

The subsequent structural integrity of the grafts (groups A–C) was also related to their integration pattern (patterns 1–3). Disorganized graft structures exhibited integration patterns similar to those of cell suspension transplants in rd1 mice (Mandai et al., 2012). Factors that contribute to the difference between patterns A and B, or between laminar interception and direct contact, have not been revealed so far and may reflect subtle differences in graft preparations or surgical injury at the time of transplantation. Generally, grafts with considerably thicker INL were often "encapsulated" by ganglion or INL cells and remained separated from the host retina (nonintegration). At the same time, group A grafts with complete INL could still integrate into the host in a direct-contact pattern, raising a question as to how these direct-contact patterns can possibly take place in the presence of graft INL. In these direct-contact patterns, the CtBP2+ photoreceptor terminals of transplanted photoreceptors in the "structured ONL" in situ were clearly associated with host bipolar dendrite tips, which differs from previous reports of successful integration of dissociated transplanted photoreceptors that made synapses after "migrating into the host ONL" (MacLaren et al., 2006). Also, the photoreceptors in a structured ONL derived from young grafts at embryonic stages could subsequently integrate into the host retina, whereas dissociated embryonic retinal progenitors were reported to have little chance to integrate and mature in host retina. This means that graft retinal sheets could provide a suitable environment for the retinal progenitors to survive and properly develop, thereby augmenting their integrating potential. Close observation of the direct-contact pattern showed that the inner part of the graft retina (other than ONL) was being "stripped off," or pushed aside, enabling the bare graft ONL cells to make a direct contact with host bipolar cells in the correct orientation (Figures S3A and S3A′). This could also imply that the graft photoreceptors in young grafts developed in a structured ONL/INL complex nearly to the stage of synaptogenesis (i.e., around

postnatal days 4–7; von Kriegstein and Schmitz, 2003), but somehow they formed host-graft synapses instead of intragraft synapses that we also observed in the neighboring area of host-graft synaptogenesis (Figures S4E–S4J). In some host-graft border area, both the host and graft bipolar cells sent dendrite terminals over the graft photoreceptor terminals of the same area. This also raises the possibility that the direct-contact integration includes a synaptic plasticity, or a synaptic switching of graft photoreceptors from the graft bipolar cells to some host bipolar cells. The event of switching, or synaptic remodeling, was also suggested in an adult photocoagulation model in rabbits, in which the neighboring photoreceptors subsequently filled in the ONL lost area to newly connect to the bipolar cells over the lesion (Gust and Reh, 2011; Sher et al., 2013). Further studies are required to determine whether there exists a preferable time window or situation for this synaptic switching to occur under the sheet transplantation conditions.

Arai et al. (2004) detected a visual response from the superior colliculus of rosetted and disorganized grafts in embryonic retinal transplantation, whereas well-organized, laminated grafts showed no response. This is consistent with our observation that synapses were found in either direct contact or cell integration, but very rarely in a laminar interception pattern. Moreover, we showed that mESC- and miPSC-derived retinal sheets could survive at least 6 months after transplantation, which is consistent with previous reports that retinal sheets could survive long periods without immune modulation (del Cerro et al., 2000; Ghosh et al., 1999; Gouras et al., 1994; Hambright et al., 2012), and suggests a greater benefit from sheet transplantations compared with cell suspensions.

In summary, retina-like sheets derived from mESCs and miPSCs are competent as a graft source for retinal sheet transplantation and are suitable for use as a clinical therapeutic strategy because (1) transplanted sheets survived well in the host retina, (2) transplanted sheets at DD17 or younger could develop to form structured ONL of mature photoreceptors in the presence of IS/OS, and (3) photoreceptors of structured ONL in the transplanted retinal sheets could form direct synaptic connections with the host bipolar cells. However, further electrophysiological examinations are warranted to confirm the presence of a light response from these grafts and their potency for transmitting the signal to the host.

EXPERIMENTAL PROCEDURES

Differentiation to 3D Retina-like Tissue from mESCs and miPSCs

The *Rx*-GFP knockin was described previously (Osakada et al., 2008; Wataya et al., 2008). *Rosa26*-tdTomato/*Rx*-GFP knockin mESCs were generated by membrane tdTomato expression construct containing a chicken b-actin promoter knocked into the *Rosa26* locus in the *Rx*-GFP cell line (Muzumdar et al., 2007). *Nrl*-GFP transgenic miPSCs generated from *Nrl*-eGFP mice (Akimoto et al., 2006; Homma et al., 2013) were maintained as previously described (Osakada et al., 2008) and differentiated into stratified neural retinas by modified serum-free floating of embryoid-body-like aggregates with quick reaggregation (SFEBq) (Eiraku et al., 2011). In brief, mESCs and miPSCs were cultured in 96-well plates at 3,000 cells/well. AGN193109 (0.1 μM, DD0–8; Toronto Research Chemicals) and growth-factor-reduced Matrigel (2% [v/v], DD1–8; BD Biosciences) were added to the differentiation medium (Glasgow minimum essential medium [G-MEM], 5% KSR [Invitrogen], 0.1 mM nonessential amino acids, 1 mM pyruvate, and 0.1 mM 2-mercaptoethanol). On DD8, optic vesicles were cut using a No. 11 blade and transferred to suspension culture under 40% O_2/5% CO_2 in Dulbecco's modified Eagle's medium (DMEM)/F-12 medium supplemented with N2 + 10% fetal bovine serum + 0.5 μM all-*trans* retinoic acid + 1 mM L-taurine. Live cells were imaged with a fluorescent inverted microscope (IX71N; Olympus).

Immunohistochemistry

Detailed procedures are described in Supplemental Experimental Procedures and the antibodies used in this study are listed in Table S1. For synaptic 3D analysis, eyes were fixed with 4% paraformaldehyde (PFA) after perfusion fixation and embedded in agarose (3% [w/v] NuSieve GTG agarose). Sections (50 μm) were made with a microtome (Leica VT-1000S) and samples were blocked with 3% Triton X-100/5% goat serum at 4°C overnight. The samples were then incubated with primary and secondary antibodies in 3% Triton X-100/5% goat serum at 4°C for two nights and overnight, respectively, and mounted with 2,2′-thiodiethanol (Sigma).

Subretinal Transplantation

All animal procedures were approved by our institutional animal experimentation committee and were in accordance with the Association for Research in Vision and Ophthalmology Statement for the Use of Animals in Ophthalmic and Vision Research. C3H/HejYokSlc (rd1) mice (6–8 weeks old) were used as graft recipients in all experiments, except for a few experiments for the detailed 3D synaptic analysis in which rd1 mice backcrossed from C3H/Hej with C57BL/6JJmsSlc for several generations were used (Figures 4J–4L). Retinal sheets were prepared from DD11–24 mESC and miPSC optic-vesicle-like spheres. Spheres were manually cut into 0.5 mm × 1.5–2 mm pieces using a No. 11 blade (Figures 2A–2D) and kept in DMEM/F-12 supplemented with N_2 on ice. The surgical transplantation procedure was done under an operating microscope. Graft-recipient mice were anesthetized by intraperitoneal injections of ketamine (7.7 mg/100 g; Daiichi Sankyo) and xylazine (0.92 mg/100 g; Bayer).

A retinal sheet was aspirated gently into a glass micropipette with a tip diameter of 500 μm. Then, the micropipette was introduced into the vitreous space through a small incision in the sclera, proceeding into the subretinal space where a retinal sheet was gently deposited (Figure 2E). All mice were kept on a standard 12 hr

light/dark cycle and were sacrificed between 2 weeks and 6 months after transplantation.

Fluorescence-Activated Cell Sorting Analysis

DD8 *Rx*-GFP mESC aggregates were dissociated with Accutase (0.25%; Invitrogen). After neutralization, the cells were resuspended in PBS with 1 μg/ml propidium iodide (PI; Sigma), and passed through a cell strainer (BD Biosciences) as described previously (Osakada et al., 2008). Cells were counted and sorted with a FACSAria (BD Biosciences) and the data were analyzed with FACSDiva software (BD Biosciences). Dead cells were excluded by PI staining.

RT-PCR

Total RNA was extracted with a QIAGEN RNeasy Plus Mini kit, and reverse transcription was completed with Superscript III (Life Technologies) treated with RNase-free DNase I and a first-strand cDNA synthesis kit (Amersham Biosciences) according to each manufacturer's protocol. Synthesized cDNA was amplified with gene-specific primers. PCR products were separated by electrophoresis on a 2% agarose gel and detected under UV illumination.

Image Acquisition for 3D Reconstruction

Retinal section images were acquired on an LSM 780 inverted confocal microscope (Zeiss) or Leica-TCS SP8. For 3D analysis, a series of XY optical sections, 0.3 μm apart, throughout the depth of the 50-μm-thick section, were taken and built into a stack to obtain sectional images. 3D reconstruction of high-resolution z-stack images was performed with Imaris software (Bitplane).

Electron Microscope Analysis

Mice were sacrificed by perfusion fixation with 4% PFA. Eyes were fixed with 2% glutaraldehyde in 4% PFA overnight. After washing with PBS, the eyes were postfixed with ice-cold 1% OsO_4 in 0.1 M sodium cacodylate buffer, pH 7.3, for 2 hr. The samples were then rinsed with distilled water, stained with 0.5% aqueous uranyl acetate for 2 hr or overnight at room temperature, dehydrated with ethanol and propylene oxide, and embedded in Poly/Bed 812 (Polyscience). Ultrathin sections were cut, double stained with uranyl acetate and Reynolds' lead citrate, and viewed with a JEM 1010 or JEM 1400 transmission electron microscope (JEOL) at an accelerating voltage of 100 kV. For further details regarding the experimental procedures used in this study, see Supplemental Experimental Procedures.

SUPPLEMENTAL INFORMATION

Supplemental Information includes Supplemental Experimental Procedures, four figures, two tables, and one movie and can be found with this article online at http://dx.doi.org/10.1016/j.stemcr.2014.03.011.

AUTHOR CONTRIBUTIONS

J.A., M.M., S.O., C.Y., and S.Y. conducted the experiments. J.A., M.M., S.Y., Y.S., and M.T. analyzed and interpreted the data. J.A., M.M., S.O., M.E., Y.S., and M.T. conceived and designed the study. J.A. and M.M. wrote the manuscript.

ACKNOWLEDGMENTS

We thank Kyoko Iseki, Tomoyo Hashiguchi, Momo Fujii, Emma West, Meng-Tsen Ke, and Takeshi Imai for technical advice; Kazuyo Misaki for electron microscope analysis; Hazuki Hiraga for proofreading the manuscript; and all members of the Takahashi Laboratory for discussion and comments. J.A. also thanks the Prince Mahidol Award Youth Program and Zi-Bing Jin for initial guidance in the experiments. This study was supported by a grant from the Research Center Network for Realization of Regenerative Medicine, MEXT.

Received: November 20, 2013
Revised: March 27, 2014
Accepted: March 27, 2014
Published: April 24, 2014

REFERENCES

Akimoto, M., Cheng, H., Zhu, D., Brzezinski, J.A., Khanna, R., Filippova, E., Oh, E.C., Jing, Y., Linares, J.L., Brooks, M., et al. (2006). Targeting of GFP to newborn rods by Nrl promoter and temporal expression profiling of flow-sorted photoreceptors. Proc. Natl. Acad. Sci. USA *103*, 3890–3895.

Arai, S., Thomas, B.B., Seiler, M.J., Aramant, R.B., Qiu, G., Mui, C., de Juan, E., and Sadda, S.R. (2004). Restoration of visual responses following transplantation of intact retinal sheets in rd mice. Exp. Eye Res. *79*, 331–341.

Barber, A.C., Hippert, C., Duran, Y., West, E.L., Bainbridge, J.W., Warre-Cornish, K., Luhmann, U.F., Lakowski, J., Sowden, J.C., Ali, R.R., and Pearson, R.A. (2013). Repair of the degenerate retina by photoreceptor transplantation. Proc. Natl. Acad. Sci. USA *110*, 354–359.

Callaerts, P., Halder, G., and Gehring, W.J. (1997). PAX-6 in development and evolution. Annu. Rev. Neurosci. *20*, 483–532.

del Cerro, M., Humayun, M.S., Sadda, S.R., Cao, J., Hayashi, N., Green, W.R., del Cerro, C., and de Juan, E., Jr. (2000). Histologic correlation of human neural retinal transplantation. Invest. Ophthalmol. Vis. Sci. *41*, 3142–3148.

Eiraku, M., Takata, N., Ishibashi, H., Kawada, M., Sakakura, E., Okuda, S., Sekiguchi, K., Adachi, T., and Sasai, Y. (2011). Self-organizing optic-cup morphogenesis in three-dimensional culture. Nature *472*, 51–56.

Ferrari, S., Di Iorio, E., Barbaro, V., Ponzin, D., Sorrentino, F.S., and Parmeggiani, F. (2011). Retinitis pigmentosa: genes and disease mechanisms. Curr. Genomics *12*, 238–249.

Furukawa, T., Kozak, C.A., and Cepko, C.L. (1997). rax, a novel paired-type homeobox gene, shows expression in the anterior neural fold and developing retina. Proc. Natl. Acad. Sci. USA *94*, 3088–3093.

Ghosh, F., Johansson, K., and Ehinger, B. (1999). Long-term full-thickness embryonic rabbit retinal transplants. Invest. Ophthalmol. Vis. Sci. *40*, 133–142.

Ghosh, F., Arnér, K., and Engelsberg, K. (2009). Isolation of photoreceptors in the cultured full-thickness fetal rat retina. Invest. Ophthalmol. Vis. Sci. *50*, 826–835.

Gonzalez-Cordero, A., West, E.L., Pearson, R.A., Duran, Y., Carvalho, L.S., Chu, C.J., Naeem, A., Blackford, S.J., Georgiadis, A., Lakowski, J., et al. (2013). Photoreceptor precursors derived from three-dimensional embryonic stem cell cultures integrate and mature within adult degenerate retina. Nat. Biotechnol. *31*, 741–747.

Gouras, P., Du, J., Kjeldbye, H., Yamamoto, S., and Zack, D.J. (1992). Reconstruction of degenerate rd mouse retina by transplantation of transgenic photoreceptors. Invest. Ophthalmol. Vis. Sci. *33*, 2579–2586.

Gouras, P., Du, J., Kjeldbye, H., Yamamoto, S., and Zack, D.J. (1994). Long-term photoreceptor transplants in dystrophic and normal mouse retina. Invest. Ophthalmol. Vis. Sci. *35*, 3145–3153.

Gust, J., and Reh, T.A. (2011). Adult donor rod photoreceptors integrate into the mature mouse retina. Invest. Ophthalmol. Vis. Sci. *52*, 5266–5272.

Hambright, D., Park, K.Y., Brooks, M., McKay, R., Swaroop, A., and Nasonkin, I.O. (2012). Long-term survival and differentiation of retinal neurons derived from human embryonic stem cell lines in un-immunosuppressed mouse retina. Mol. Vis. *18*, 920–936.

Hirami, Y., Osakada, F., Takahashi, K., Okita, K., Yamanaka, S., Ikeda, H., Yoshimura, N., and Takahashi, M. (2009). Generation of retinal cells from mouse and human induced pluripotent stem cells. Neurosci. Lett. *458*, 126–131.

Homma, K., Okamoto, S., Mandai, M., Gotoh, N., Rajasimha, H.K., Chang, Y.S., Chen, S., Li, W., Cogliati, T., Swaroop, A., and Takahashi, M. (2013). Developing rods transplanted into the degenerating retina of Crx-knockout mice exhibit neural activity similar to native photoreceptors. Stem Cells *31*, 1149–1159.

Humayun, M.S., Dorn, J.D., da Cruz, L., Dagnelie, G., Sahel, J.A., Stanga, P.E., Cideciyan, A.V., Duncan, J.L., Eliott, D., Filley, E., et al.; Argus II Study Group (2012). Interim results from the international trial of Second Sight's visual prosthesis. Ophthalmology *119*, 779–788.

Ikeda, H., Osakada, F., Watanabe, K., Mizuseki, K., Haraguchi, T., Miyoshi, H., Kamiya, D., Honda, Y., Sasai, N., Yoshimura, N., et al. (2005). Generation of Rx+/Pax6+ neural retinal precursors from embryonic stem cells. Proc. Natl. Acad. Sci. USA *102*, 11331–11336.

Jacobson, S.G., Cideciyan, A.V., Ratnakaram, R., Heon, E., Schwartz, S.B., Roman, A.J., Peden, M.C., Aleman, T.S., Boye, S.L., Sumaroka, A., et al. (2012). Gene therapy for Leber congenital amaurosis caused by RPE65 mutations: safety and efficacy in 15 children and adults followed up to 3 years. Arch. Ophthalmol. *130*, 9–24.

Lamba, D.A., Karl, M.O., Ware, C.B., and Reh, T.A. (2006). Efficient generation of retinal progenitor cells from human embryonic stem cells. Proc. Natl. Acad. Sci. USA *103*, 12769–12774.

Lamba, D.A., Gust, J., and Reh, T.A. (2009). Transplantation of human embryonic stem cell-derived photoreceptors restores some visual function in Crx-deficient mice. Cell Stem Cell *4*, 73–79.

Lamba, D.A., McUsic, A., Hirata, R.K., Wang, P.R., Russell, D., and Reh, T.A. (2010). Generation, purification and transplantation of photoreceptors derived from human induced pluripotent stem cells. PLoS ONE *5*, e8763.

Lolley, R.N., Rong, H., and Craft, C.M. (1994). Linkage of photoreceptor degeneration by apoptosis with inherited defect in phototransduction. Invest. Ophthalmol. Vis. Sci. *35*, 358–362.

MacLaren, R.E., Pearson, R.A., MacNeil, A., Douglas, R.H., Salt, T.E., Akimoto, M., Swaroop, A., Sowden, J.C., and Ali, R.R. (2006). Retinal repair by transplantation of photoreceptor precursors. Nature *444*, 203–207.

Mandai, M., Homma, K., Okamoto, S., Yamada, C., Nomori, A., and Takahashi, M. (2012). Adequate time window and environmental factors supporting retinal graft cell survival in *rd* mice. Cell Med. *4*, 45–54.

Meyer, J.S., Shearer, R.L., Capowski, E.E., Wright, L.S., Wallace, K.A., McMillan, E.L., Zhang, S.C., and Gamm, D.M. (2009). Modeling early retinal development with human embryonic and induced pluripotent stem cells. Proc. Natl. Acad. Sci. USA *106*, 16698–16703.

Muzumdar, M.D., Tasic, B., Miyamichi, K., Li, L., and Luo, L. (2007). A global double-fluorescent Cre reporter mouse. Genesis *45*, 593–605.

Osakada, F., Ikeda, H., Mandai, M., Wataya, T., Watanabe, K., Yoshimura, N., Akaike, A., Sasai, Y., and Takahashi, M. (2008). Toward the generation of rod and cone photoreceptors from mouse, monkey and human embryonic stem cells. Nat. Biotechnol. *26*, 215–224.

Pearson, R.A., Barber, A.C., Rizzi, M., Hippert, C., Xue, T., West, E.L., Duran, Y., Smith, A.J., Chuang, J.Z., Azam, S.A., et al. (2012). Restoration of vision after transplantation of photoreceptors. Nature *485*, 99–103.

Schmitz, F., Königstorfer, A., and Südhof, T.C. (2000). RIBEYE, a component of synaptic ribbons: a protein's journey through evolution provides insight into synaptic ribbon function. Neuron *28*, 857–872.

Seiler, M.J., and Aramant, R.B. (1998). Intact sheets of fetal retina transplanted to restore damaged rat retinas. Invest. Ophthalmol. Vis. Sci. *39*, 2121–2131.

Sharma, R.K., O'Leary, T.E., Fields, C.M., and Johnson, D.A. (2003). Development of the outer retina in the mouse. Brain Res. Dev. Brain Res. *145*, 93–105.

Sher, A., Jones, B.W., Huie, P., Paulus, Y.M., Lavinsky, D., Leung, L.S., Nomoto, H., Beier, C., Marc, R.E., and Palanker, D. (2013). Restoration of retinal structure and function after selective photocoagulation. J. Neurosci. *33*, 6800–6808.

Singh, M.S., Charbel Issa, P., Butler, R., Martin, C., Lipinski, D.M., Sekaran, S., Barnard, A.R., and MacLaren, R.E. (2013). Reversal of end-stage retinal degeneration and restoration of visual function by photoreceptor transplantation. Proc. Natl. Acad. Sci. USA *110*, 1101–1106.

Strissel, K.J., Lishko, P.V., Trieu, L.H., Kennedy, M.J., Hurley, J.B., and Arshavsky, V.Y. (2005). Recoverin undergoes light-dependent intracellular translocation in rod photoreceptors. J. Biol. Chem. *280*, 29250–29255.

Takahashi, K., and Yamanaka, S. (2006). Induction of pluripotent stem cells from mouse embryonic and adult fibroblast cultures by defined factors. Cell *126*, 663–676.

von Kriegstein, K., and Schmitz, F. (2003). The expression pattern and assembly profile of synaptic membrane proteins in ribbon synapses of the developing mouse retina. Cell Tissue Res. *311*, 159–173.

Wataya, T., Ando, S., Muguruma, K., Ikeda, H., Watanabe, K., Eiraku, M., Kawada, M., Takahashi, J., Hashimoto, N., and Sasai, Y. (2008). Minimization of exogenous signals in ES cell culture induces rostral hypothalamic differentiation. Proc. Natl. Acad. Sci. USA *105*, 11796–11801.

West, E.L., Pearson, R.A., Barker, S.E., Luhmann, U.F., Maclaren, R.E., Barber, A.C., Duran, Y., Smith, A.J., Sowden, J.C., and Ali, R.R. (2010). Long-term survival of photoreceptors transplanted into the adult murine neural retina requires immune modulation. Stem Cells *28*, 1997–2007.

Stem Cell Reports, Volume *2*

Supplemental Information

Transplantation of Embryonic and Induced Pluripotent Stem Cell-Derived 3D Retinal Sheets into Retinal Degenerative Mice

Juthaporn Assawachananont, Michiko Mandai, Satoshi Okamoto, Chikako Yamada, Mototsugu Eiraku, Shigenobu Yonemura, Yoshiki Sasai, and Masayo Takahashi

INVENTORY OF SUPPLEMENTARY INFORMATION

Supplementary movie: 1

Movie S1, related to Fig. 4.

Supplementary figures: 4

Figure S1. Characterization of mESC- and miPSC-derived 3D retina, related to Fig.1

Figure S2. Sub sequential outcome of retinal grafts in rd1 subretinal space, related to Fig.2

Figure S3. Host-graft integration, related to Fig.4

Figure S4. Ribbon synaptic formation, related to Fig.4

Supplementary tables: 2

TableS1. Primary antibodies and their working dilutions, related to Fig. 1-4 and Fig. S1-4

Table S2. Reverse transcriptase-polymerase chain reaction (RT-PCR) primer, related to Fig. 1

Supplementary experimental procedures

Figure S1. Characterization of mESC- and miPSC-derived 3D retina, related to Fig.1

A) DD.9 *Rx*-GFP mESC-derived sphere showed PAX6-*Rx* positive in optic vesicle-like structure and PAX6 also expressed in part of the rest. **B)** Comparative immunostaining pattern of mESC- and iPSC-derived retina and neonatal mouse retina. CRX (photoreceptor-specific transcription factor), RECOVERIN, (calcium binding protein inhibitor of rhodopsin kinase), CALRETININ (calcium binding protein, labeled Amacrine and Ganglion cells) and RHODOPSIN. **C)** *Nrl*-GFP iPSC-derived retina from DD.15 to DD.30 gradually expressed GFP along the differentiation time course (All photos had been taken with same exposure). Scale bars: 500 µm(**C**), 100 µm(**A**), 50 µm(**B**).

Figure S2. Sub sequential outcome of retinal grafts in rd1 subretinal space, related to Fig.2

A) Graph shows subsequent differentiation patterns of transplanted sheets of each DD. categorized into three groups; Group A: Retinal sheet with inner nuclear layer (INL)/ inner plexiform layer (IPL) and ONL (**Fig.2H-K**), Group B: Retinal sheet with ONL and the remaining INL cells (**Fig.2L**) and Group C: Disorganized structure (**Fig.2M**). **B)** Diagram shows degree of maturation and structural integrity of young grafts (DD.11-17) post-transplantation in short (2-4 weeks), mid (1-3 months) and long (>3months) term. **C)** DD.16 *Rx*-GFP mESC-derived retinal sheet with structured outer nuclear layer and IS/OS survived up to 6 months in rd subretinal space. Scale bars: 200 µm (**C**)

Figure S3. Host-graft integration, related to Fig.4

A-A') DD.16 *Nrl*-GFP miPSC-derived retinal sheet was in direct contact pattern with host retina. Graft ONL were managed to come in direct contact with the host cells (black and white dashed

arrowhead line in **A** and **A'** respectively). The inner part of the grafts (INL/IPL) were stripped off (yellow arrowhead line) from the graft ONL and graft bipolar cells were push aside (red dashed arrowhead line) when the exposed ONL part formed a direct contact with the host cells (same samples as **Fig.2L**). **B)** Comparison of graft integration patterns between miPSC-derived retina (*Nrl*-GFP miPSC line) and mESC-derived retina (*Rx*-GFP mESC line) of the young grafts (DD.11-17) and older grafts (DD.18-24). **C)** DD.13 Rosa26-TdTomato *Rx*-GFP mESC-derived retinal grafts showed integration into host retinas; both host bipolar (PKC-α) and graft cells (Rosa26-TdTomato) extended processes across the area of host-graft interface, and graft cells were not migrating into the host retina. **D-D')** DD.13 *Rx*-GFP mESC-derived retinal graft with direct contact pattern showed synaptic connection between host and graft interface (white dashed line). Host bipolar (PKC-α positive, *Rx*-GFP negative) were co-labeled with CtBP2 (yellow arrow) and graft photoreceptor (*Rx*-GFP-positive with dense chromatin of rod nuclei; **D'**) **E)** DD.21 *Nrl*-GFP miPSC-derived retinal graft in disorganized pattern also showed host bipolar tip (asterisk, PKC-α) labeled with synapses (CtBP2, yellow arrow head) in host-graft interface area (white dashed line). **F)** Muller glia from host and graft of DD.16 *Nrl*-GFP miPSC-derived retinal graft with Pattern 2 (same samples as **Fig.2L** and **Fig. S3A-A'**) **G)** Muller glia from host and graft of DD.18 *Rx*-GFP mESC derived retinal graft with Pattern 3 (same samples as **Fig.2I** and **4C**). Scale bars: 200 μm (**A**), 50 μm (**A',F,G**), 20 μm (**C**), 10 μm (**E**), 5 μm (**D**).

Figure S4. Ribbon synaptic formation, related to Fig.4

A-A') DD.18 *Rx*-GFP: Rosa26-TdTomato mESC-derived retinal graft showed structured ONL integrated to host retina with a direct contact pattern with OS towards RPE. **B-D**) Electron micrographs from DD.18 Rosa26-TdTomato *Rx*-GFP mESC-derived retinal grafts same samples as in **A-A'**. Some of the synaptic sites with ribbon structure were indicated along host-graft interface (red arrow head; **B'**). Higher magnification images showed rod spherule (red arrow; **C, same as in Fig.4M**). Ribbon synapses were detected in the area of host-graft interface (**D1-4**). **E-G,** DD.14 *Nrl*-GFP miPSC-derived retinal sheet developed stratified neural retina that happened to locate continuously in the break of the host retina (**E**). Host-graft junction; white arrow head (**F**). Intra-graft synapses were identified by immunostaining of PKC-α and presynaptic protein, Bassoon. (**G**). **H-J,** Electron micrographs of intra-graft typical rod photoreceptor ribbon spherule (black arrowhead) from DD.17 *Nrl*-GFP miPSC-derived retina. (**H,J**), **I** higher magnification of **H**. H; host, G; graft, IPL; inner plexiform layer, INL; inner nuclear layer, OPL; outer plexiform layer, ONL; outer nuclear layer, RB; rod bipolar, H; horizontal cells; OS; outer segment, RPE; retinal pigment epithelium. Scale bars: 100 µm (**E**), 50 µm (**A,A'**), 10 µm (**B, G**), 20 µm (**F**), 2 µm (**H**), 1 µm (**C ,J**), 500 nm (**I**), 200 nm (**D1-4**).

Figure S1. Characterization of mESC- and miPSC-derived 3D retina, related to Fig.1

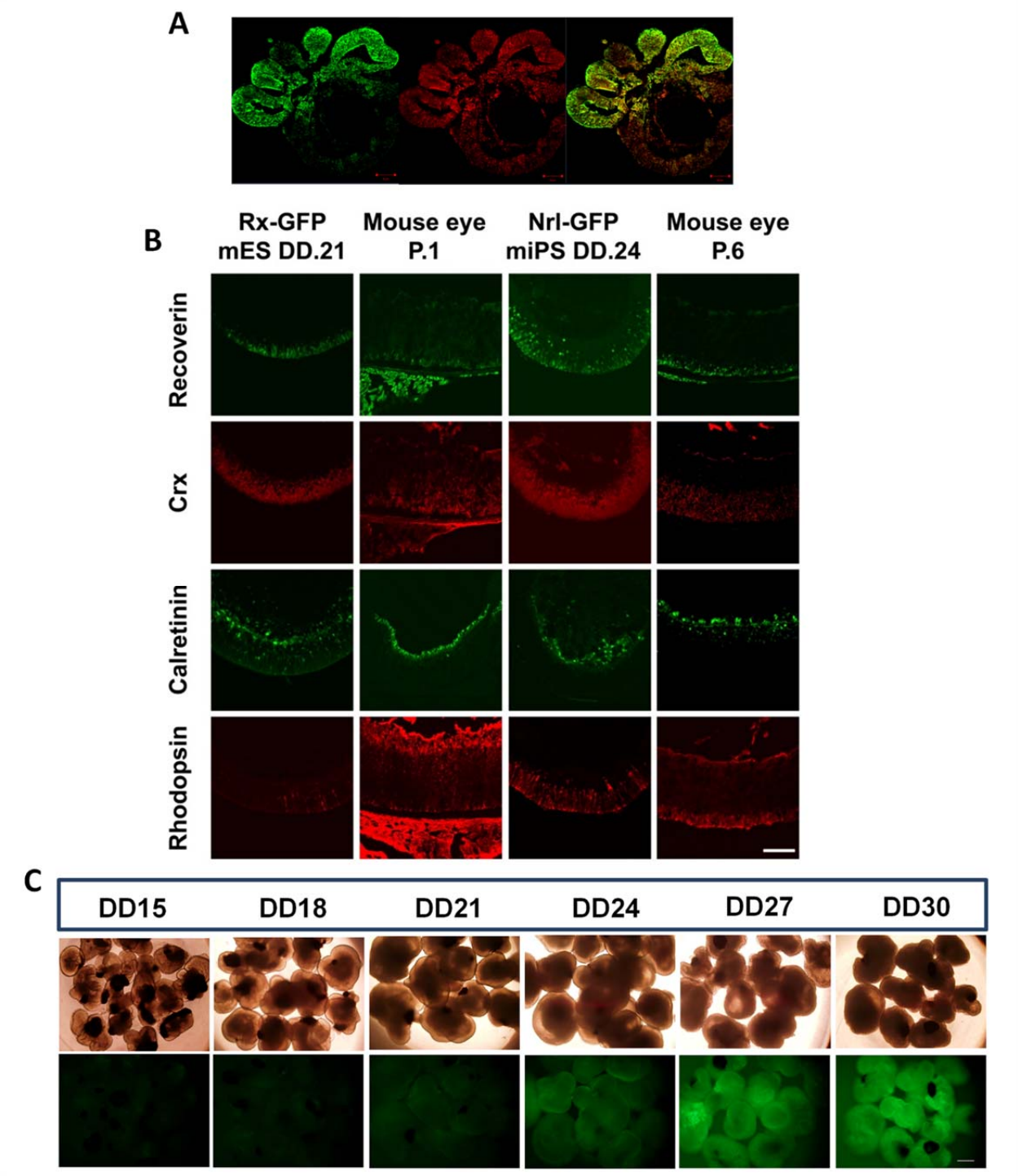

Figure S2. Sub sequential outcome of retinal grafts in rd1 subretinal space, related to Fig.2

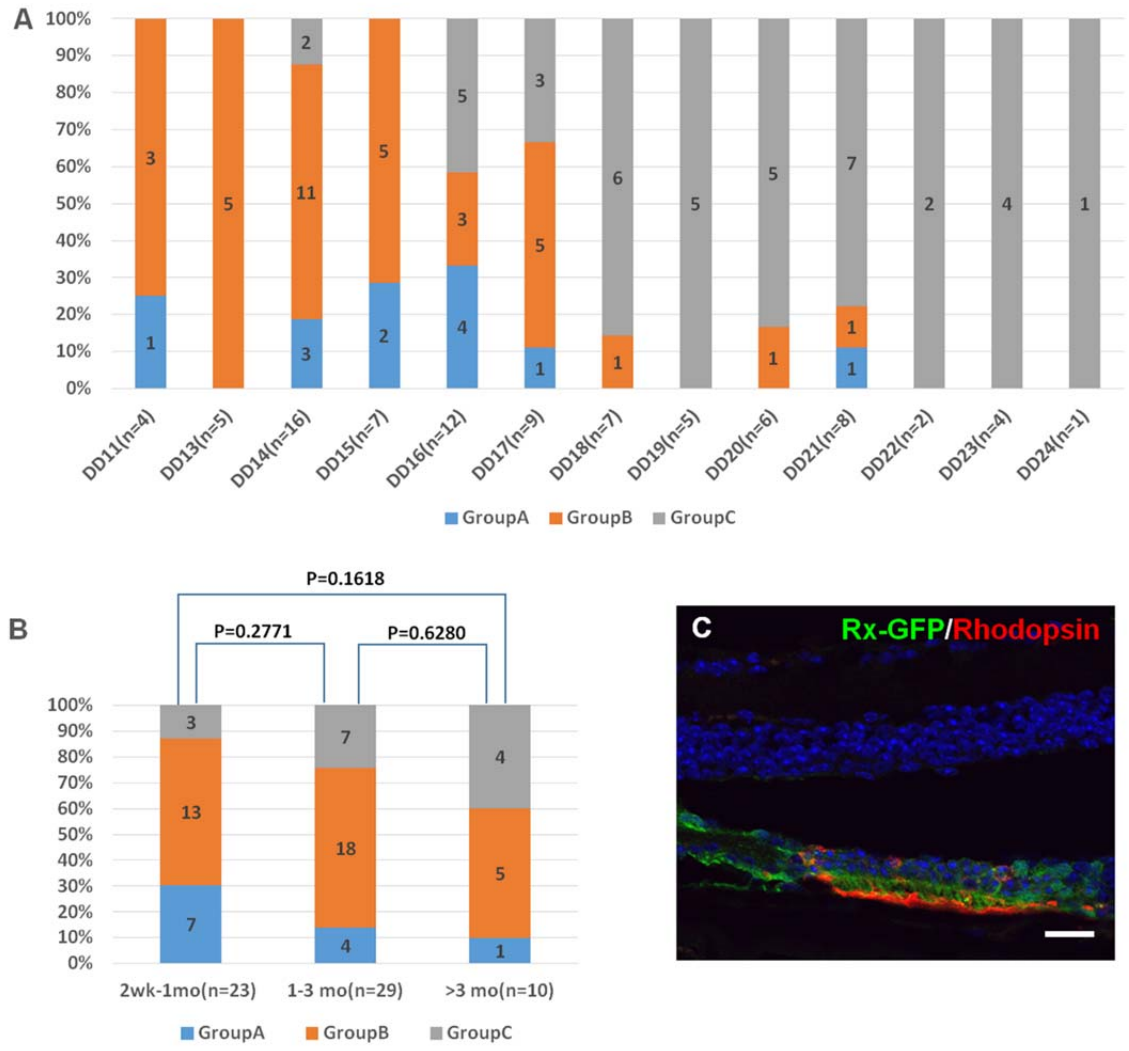

Figure S3. Host-graft integration, related to Fig.4

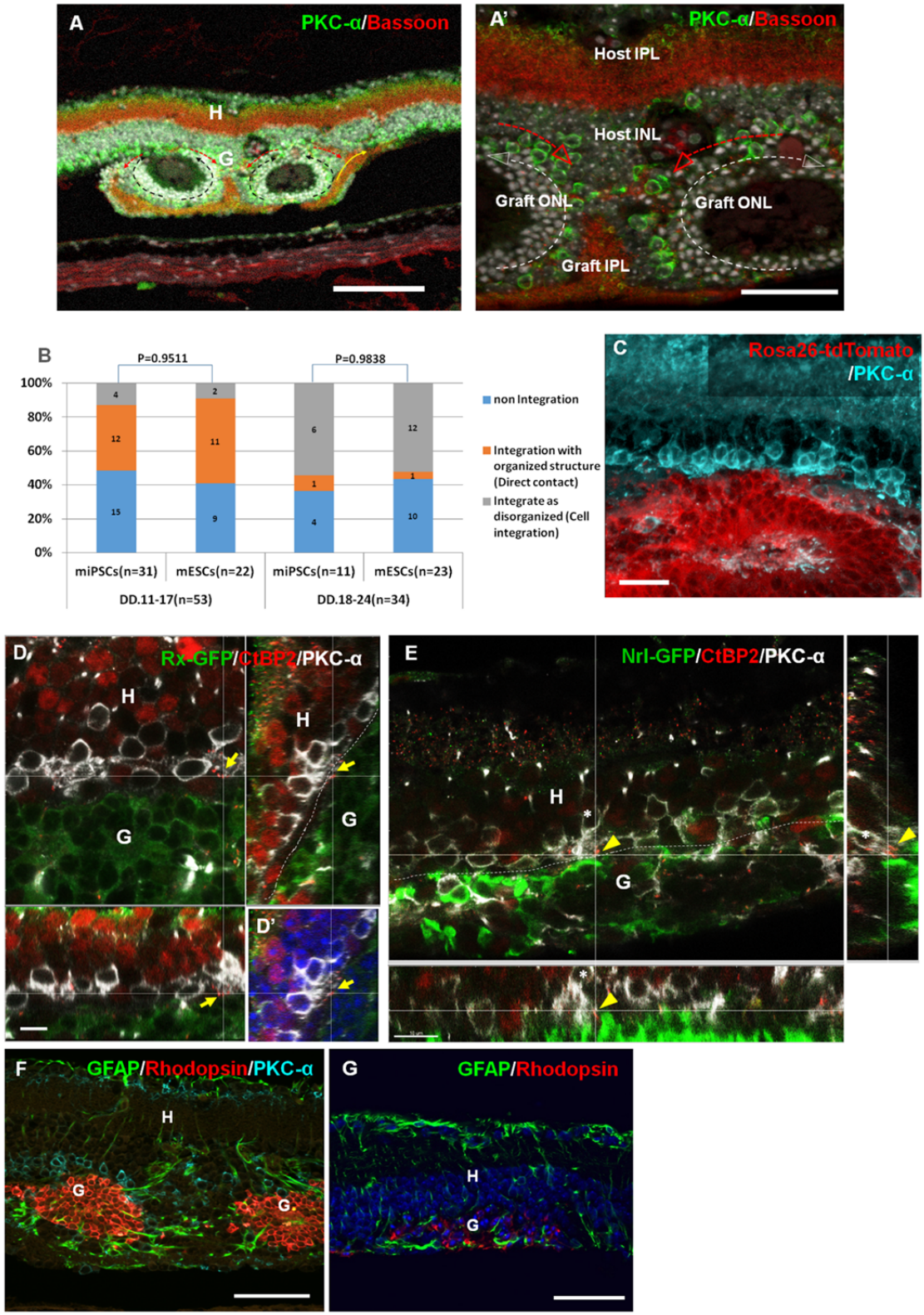

Figure S4. Ribbon synaptic formation, related to Fig.4

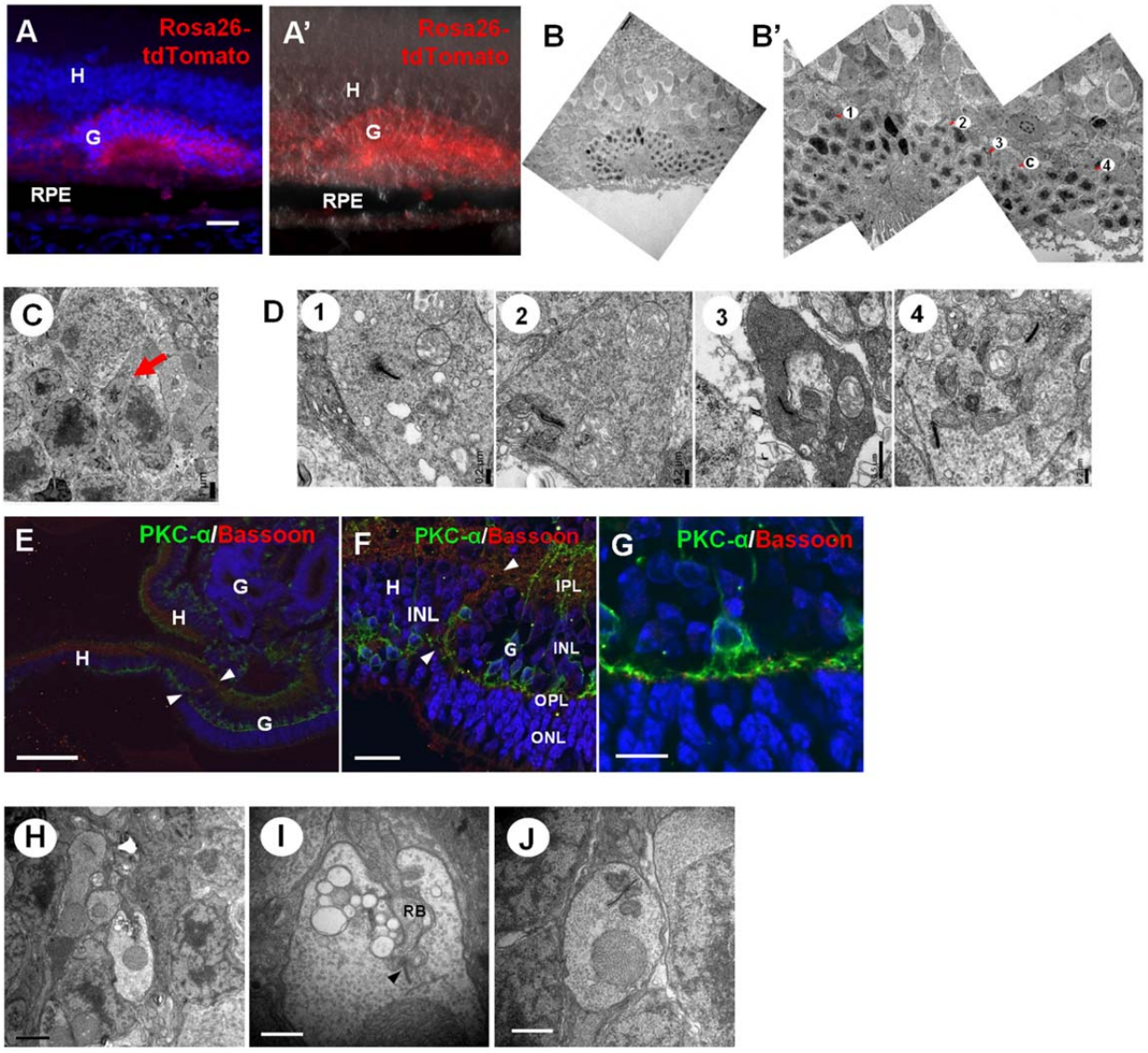

Table S1. Primary antibodies and their working dilutions

Gene	**Forward primer sequence**	**Reverse primer sequence**
Rx	GGAACCTCCCAAGAAGAAGC	GGAACCTCCCAAGAAGAAGC
Oct4	TCTTTCCACCAGGCCCCCGGCTC	TCTTTCCACCAGGCCCCCGGCTC
Nanog	AGGGTCTGCTACTGAGATGCTCTG	CAACCACTGGTTTTTCTGCCACCG
G3phd	ACCACAGTCCATGCCATCAC	TCCACCACCCTGTTGCTGTA

Table S2. Reverse transcriptase-polymerase chain reaction (RT-PCR) primer, related to Fig. 1.

Antibody	**Species**	**Dilution**	**Company**
anti-BRN3A	mouse	1:600	Chemicon
anti-CALBINDIN	rabbit	1:1000	Chemicon
anti-CALRETININ	rabbit	1:1000	Chemicon
anti-CRX	mouse	1:1000	Abnova
anti-CtBP2	mouse	1:500	BD Bioscience
anti-DsRed	mouse	1:500	Clontech
anti-ISLET1/2	mouse	1:200	Developmental Studies Hybridoma Bank
anti-GFAP	mouse	1:1000	Chemicon
anti-GFP	rabbit	1:1000	Invitrogen
anti-GFP	rat	1:1000	Nacalai
anti-GS	mouse	1:1000	Chemicon
anti-LAMININ	rabbit	1:200	Abcam

anti-PAX6	mouse	1:1000	Cosmo Bio. Co
anti-PKCα	mouse	1: 1000	Sigma
anti-PKCα	rabbit	1:1000	Sigma
anti-RECOVERIN	rabbit	1:1000	Millipore
anti-RHODOPSIN(RET-P1)	mouse	1:1000	Sigma
anti-ZO-1	rabbit	1:100	Zymed

Supplementary experimental procedures

Immunocytochemistry

Aggregates or eyes were fixed with 4% paraformaldehyde, washed with PBS, and cryoprotected in 10% sucrose in PBS for 1hr and 30% sucrose in PBS overnight at 4°C.Then they were embedded in OCT (Tissue Tec; Sakura Finetechnical Co) and frozen in -180° C. Then embedded aggregates or eyes were cryosectioned with cryostat (HM560; Thermo).

Eyes were enucleated and placed in fixative (SUPERFIX, Kurabo, Osaka, Japan) at 4°C overnight. After automatic fixation (Excelsior, ThermoFisher Co., UK), the eyes were embedded in paraffin (P3683; Sigma, St.Louis, MO) and the paraffin blocks were sectioned using an autoslide preparation system (AS-200, Kurabo, Osaka, Japan)(Mandai, Homma et al. 2012).

Specimens were permeabilized 0.3% Triton X-100 in PBS for 45 min at room temperature, blocked with goat serum for 1 hr at room temperature, and incubated with the primary antibody (Table S.1) overnight at 4°C followed by secondary antibody reactions for 1-2 hr at room temperature. The secondary antibodies used were as follows: Anti-mouse Alexa fluoro 488, 546, 647 (1:1000, Molecular Probe), Anti-rabbit Alexa fluoro 488, 546, 647 (1:1000, Molecular Probe) and Anti-rat Alexa fluoro 488 (1:1000, Molecular Probe).

The immunoreactivity of each antibody was confirmed by immunostaining with appropriate retinal tissues as a positive control under the same conditions.

Cell nuclei were counterstained with 4',6-diamidino-2-phenylindole (DAPI; 1 µg/ml, Molecular Probes). Labeled cells were imaged with a Confocal microscopes LSM 510 (Zeiss), Leica-TCS SP8, LSM 710, inverted (Zeiss) or Confocal microscope LSM 780, inverted (Zeiss)

Mandai, M., K. Homma, et al. (2012). "Adequate Time Window and Environmental Factors Supporting Retinal Graft Cell Survival in rd Mice." Cell Medicine **4**: 45-54. .